Algorithm Theoretical Basis Document

ATBD 2.4

RETRIEVAL OF TOTAL WATER VAPOUR CONTENT FROM MERIS MEASUREMENTS

J. Fischer and R. Bennartz

Freie Universität Berlin

Contents

1. Introduction

1.1 Algorithm identification

MERIS.RRGVWC

1.2 Introduction

Water vapour is the most effective greenhouse gas in the atmosphere. It influences weather and climate and is responsible for clouds developement, precipitation, and modulates the atmospheric radiative energy transfer (Ramanathan *et al.*, 1989). Therefore it influences the energy balance of the earth and thus also temperature and circulation of the earth-atmosphere system (Starr and Melfi, 1991).

Water vapour varies strongly in time and space leading to the necessity of a global monitoring of atmospheric water vapour content from satellites. Today, operational satellite detection of total water vapour using a passive microwave sensor are carried out with SSM/I (**S**pecial **S**ensor **M**icrowave **I**mager) with a mean error in the column content of 7 % (Schlüssel and Emery, 1990). The spatial resolution is 49 *km* x 63 *km* is not sufficient to obtain full mesoscale water vapour information. The presence of clouds does not limit the retrieval with microwave sensors. Microwave retrieval algorithms, however, are limited to low emissivity water surfaces.

The water vapour retrieval above land surfaces with current satellite sensors is more difficult. With HIRS-2 (High Resolution Infrared Sounder), a part of TOVS (**T**iros-N **O**perational **V**ertical **S**ounder), a polar orbiting infrared-microwave sensor on board the NOAA satellites, total water vapour content above land surfaces is determined by using 5 spectral channels between 6 and 14 μm with a relative error of 20 % (Susskind *et al.*, 1984, Starr/Melfi, 1991). Inaccuracies arise due to the required estimation of the temperature and water vapour profiles as well as surface temperature (Gao, 1993). Again, the spatial resolution is not sufficient for mesoscale water vapour studies. Additionally the application is limited to clear sky conditions.

Besides HIRS-2, the VISSR (Visible-Infrared Spin Scan Radiometer) atmospheric sounders VAS (VISSR Atmospheric Sounder) on board of the geostationary satellites GOES (Geostationary Operational Environmental Satellite) and METEOSAT measure the total water vapour content (Starr and Melfi, 1991) in the infrared spectral range. However, there are similar restrictions as for HIRS-2 measurements (Hayden, 1988). The estimation of errors is limited due to the strong spatial variability of water vapour: A comparisons of radiosonde with low resolution data is difficult (Starr and Melfi, 1991). Chesters (1983) compared radiosonde data with GOES/VAS measurements and indicates an accuracy of 1 g/cm^2 in the water vapour range between 1.7 and 5.5 g/cm^2.

Furthermore, water vapour column content retrieval algorithms have been proposed for aircraft or satellite measurements using absorption of solar radiation in the $\rho\sigma\tau$ water vapour absorption band around 1 μm. Fischer (1989) proposed a differential absorption method using two spectral bands within a small interval to minimize the influence of spectrally varying surface reflectances. The spectral region between λ = 880 and λ = *905 nm* was found to be most appropriate for the retrieval of the total water vapour content, even for dry atmospheres. The spectral bandwidth of the channels should not exceed $\Delta\lambda = 10\ nm$. An accuracy of 10 % was predicted above a wide range of natural surfaces (Bowker *et al.*, 1985), if the variation of the surface reflectance is unknown within the algorithm.

Gao and Goetz (1990) were the first to use experimental data to demonstrate that the columnar water vapour content can be retrieved from airborne imaging spectrometers. Gao *et al.* (1993) proposed at least three spectral channels for the American spectrometer MODIS on board of the EOS platform, scheduled for launch in 1998: one broadband channel around *940 nm* and two narrow band channels in the window regions located near the short- and longwave edges of the ρστ absorption band. The spectral slope of surface reflectivity and atmospheric scattering are assumed to be linear between the two window channels. The estimated relative error of retrieved water vapour is about *5 %* for visibilities above 20 *km*. The error due to spectral nonlinear variations of surface reflectivity is less than *8 %*.

The algorithm of Frouin *et al.* (1990) uses two spectral channels both centred around 935 *nm* but with different bandwidths. Comparisons with radiosonde data show 15 % relative error when calculating the total water vapour column content from measured downward radiance. The measurements were ground-based, where the influence of surface reflectivity can be neglected. Aircraft measurements of up-welling solar radiance during two flights yielded 13 % and 18 % relative error, respectively. Neither spectral non-linearities of atmospheric scattering parameters nor those of the surface reflectance were taken into account.

The French POLDER (POLarization and Directionality of Earth Reflectances) on board the Japanese satellite ADEOS (ADvanced Earth Observing Satellite), which has been launched 1996, measured total water vapour by using two spectral channels (865 *nm*, spectral bandwidth 40 *nm*, and 910 *nm*, spectral bandwidth 20 *nm*) with an expected relative error of approximately 10 %. The advantage of the same center wavelength in Frouin’s algorithm, concerning variations of optical parameters between the two channels, is lost.

The MERIS instrument will have two channels for the water vapour measurement, located at *890 nm* and *900 nm*, both with *10 nm* bandwidth. As previously demonstrated by Bartsch *et al.* (1997), this channel setting minimizes the effects of surface albedo slope, whereby the channel location at the shortwave edge of the ρστ absorption band yields a good sensor response.

The following investigation focuses on the retrieval of total water vapour mainly above land surfaces. Investigations of water vapour retrieval above water surfaces as well as above clouds are included. Above water surfaces the total water vapour determination is restricted by the low reflectance. Outside the region of the sun glitter, the influence of aerosols and the interaction of aerosol scattering and water vapour absorption governs the signal. The water vapour algorithm over ocean accounts for the aerosol scattering by including the MERIS ‘aerosol’ channels 9, 12, and 13.

2 Algorithm overview

The water vapour retrieval algorithms dedicated for MERIS are based on the work of Fischer (1989), Bartsch, (1996) and Bartsch *et al.* (1997). The general algorithm approach is to relate the columnar water vapour content to the ratio of MERIS channels 14 and 15, located at 890 nm and 900 nm, respectively. The general form of the retrieval algorithms is

$$W = k_0 + k_1 \log(\tfrac{L_{Ch15}}{L_{Ch14}}) + k_2 \log^2(\tfrac{L_{Ch15}}{L_{Ch14}}), \quad (1)$$

where W is the column amount of water vapour, L_{CH14} and L_{CH15} are the radiances measured in MERIS channels 14 and 15, and k_0, k_1 and k_2 are regression constants. This simple model is based on the assumption that a logarithmical relation between the absorber mass and extinction exists. It therefore reflects Lamberts law for an idealized non-scattering atmosphere, unsaturated absorption and monochromatic radiation. Since none of these preconditions are perfectly given, an empirical quadratic correction term is introduced in Equation (1). It has to be outlined that the model described into Equation (1) has been chosen because of its simplicity and its physical motivation. The relation between W and the radiance ratio may be fitted by several other non-linear functions with similar results in terms of the retrieval error.

The regression coefficients are derived by inverting results of the below described radiative transfer model MOMO. In any case the regression constants depend on observation geometry. For the ocean algorithm they additionally depend on aerosol optical depth, derived from MERIS' atmospheric correction channels 9, 12, and 13. For land surfaces, the regression constants additionally depend on surface pressure, since pressure variations cause variations in water vapour absorption due to the pressure broadening of the absorption lines.
The derivation of the regression constants along with a description of MOMO and of the performed radiative transfer simulations may be found in section 3. Technical details of the algorithm implementation may also be found in section 3. Section 4 is dedicated to a detailed error analysis, taking into account variations of atmospheric parameters, spectral surface albedo slope, sensor noise, and observation geometry.

3 Algorithm description

3.1 Theoretical description

3.1.1 Physical basis

3.1.1.1 General

Within the solar spectral range the $\rho\sigma\tau$-band around 935 nm exhibits strong absorption by water vapour. The transmission for two model atmospheres within the spectral range relevant for MERIS channel 15 is shown in Figure 3-1. The strength and broadness of individual lines is controlled by total water vapour amount, pressure, and temperature variations. Variations in atmospheric transmission directly translate to variations in the measured radiance. Over land surfaces the magnitude of the measured signal is mainly governed by variations of surface reflectance. Independence of surface albedo is gained relying on radiance ratios between MERIS channel 15 and the almost absorption-free reference channel 14. The assumption is, that scattering and absorption properties of other atmospheric constituents and the surface albedo do not differ significantly for these two channels. This presumption is crucial for the successful retrieval of water vapour. It is shown that for the majority of measurements the presumption is fulfilled to a high accuracy. This confirms results of earlier studies (Bartsch *et al.*, 1997), namely that the choice of the MERIS water vapour channels is optimal to minimize this effect. For cases where surface albedo differs significantly between channel 14 and 15 a simple correction algorithm is proposed.

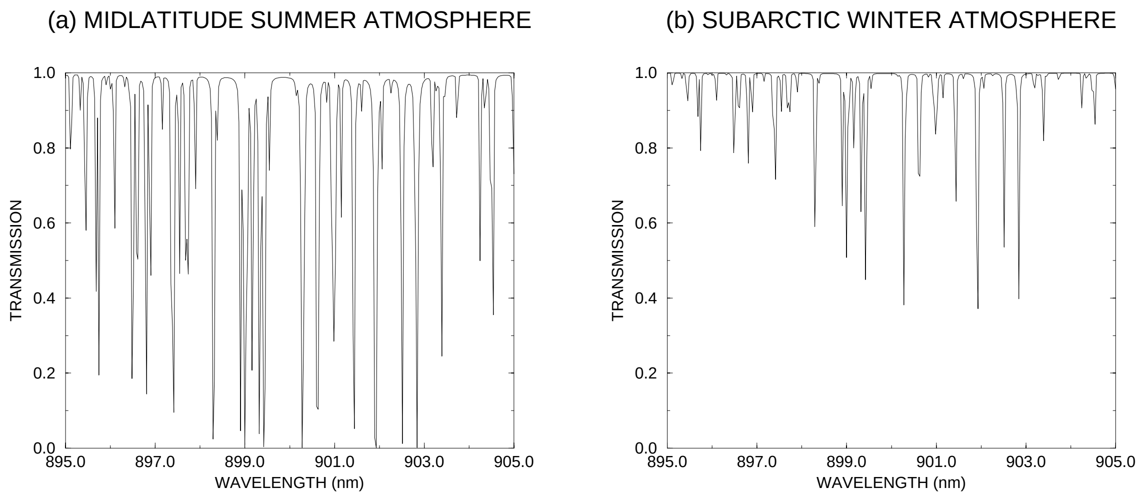

Figure 3.1: Atmospheric transmission between 895nm and 905nm for two standard atmospheres, calculated from the HITRAN-96 database

Outside the sun glitter water surfaces show a significantly lower surface reflectivity at higher wavelengths. The measured signal over water surfaces is mainly governed by aerosol scattering. Even though the overall structure of the ocean algorithm described by Equation (1) holds, the underlying physics differs significantly from the land algorithm. The effects of variable aerosol optical depth and of variations in aerosol and water vapour vertical profiles are the most significant factors affecting the retrieval accuracy. This has been accounted for by introducing a dependence of the regression coefficients on the aerosol optical depth. Despite this correction, the retrieval accuracy of the ocean algorithm, outside the sun glitter, is still inferior to that over land surfaces.

The sun glitter region has to be treated separately within the retrieval algorithm for water surfaces. Within the sun glitter region, the measured signal is comparable to that above land surfaces and hence land algorithms may be applied. The accuracy of retrievals over sun glitter is expected to be comparable to land surfaces.

Clouds are bright targets with small spectral variation in reflectivity. Water vapour retrieval results under cloudy conditions are therefore expected to be feasible. Variations in penetration depth of the incoming solar radiation lead to uncertainties in the assignment of the measured water vapour content to an altitude range. The penetration depth is mainly governed by the ratio between cloud optical depth and cloud geometrical thickness. The issues associated with variable penetration depth are closely related to cloud top pressure retrieval and are discussed in more detail in the cloud top pressure ATBD. Another factor, limiting the retrieval accuracy, is the comparably low water vapour content available above high clouds which generally leads to an increasing relative errors with increasing cloud top height.

3.1.1.2 Algorithm development

The algorithms provided are based on inverse radiative transfer modelling. A large dataset of different atmospheric profiles of water vapour, temperature, pressure, and aerosol types and vertical distributions are used as input parameters for the radiative transfer simulations. This input dataset virtually covers the global variability of these parameters. From the simulated radiance ratios regression coefficients are derived for all combinations of independent input variables, namely, sun- and observer zenith angle, relative azimuth, and aerosol optical depth. In the subsequent sections the radiative transfer model as well as the physical input parameters for the simulations are described.

3.1.1.2.1 Matrix Operator Model (MOMO)

The radiative transfer code MOMO (Fischer and Graßl, 1983; Fell and Fischer, 1995) is used to simulate the radiances for the MERIS channels. The Matrix Operator Method (Plass *et al.*, 1973) offers the possibility of a) combination of layers of any given optical properties b) very fast calculation even in the case of optically thick layers with highly anisotropic phase functions c) choice of any desired surface reflectivity, and d) the calculation of up- and down-welling radiances within the ocean and the atmosphere for all layer boundaries.
Scattering and absorption processes due to aerosols and cloud particles are represented by appropriate scattering and extinction coefficients and the corresponding scattering phase function. These parameters are obtained by Mie theory. Air molecules are small compared to the wavelength of the incoming sunlight. Thus the molecular scattering can be described with Rayleigh theory.

The exponential sum fitting technique for transmission (ESFT) is employed to incorporate absorption by gases (Armbruster and Fischer, 1995). The approximation of transmission functions with exponential sums is used for the spectral integration within the radiative transfer code. The calculation of the gas absorption is based on the HITRAN dataset

(Rothman *et al.*, 1992), which contains parameters of the single absorption lines of the main atmospheric gases.

The model has extensively been validated by comparisons with Monte-Carlo-models (Heinemann and Gentili, 1995) and with airborne radiation measurements (Schüller *et al.*, 1997).

3.1.1.2.2 Radiative transfer simulations for the algorithm development

A number of 432 azimuthally resolved radiance spectra were calculated, covering a broad range of atmospheric temperature and pressure profiles, aerosol optical depths, surface reflectivities and total water vapour content both, over land and water surfaces. The vertical structure of the atmosphere was described by 20 homogeneous model layers. The input parameters of the simulations are described in detail in the following sections.

3.1.1.2.3 Vertical temperature, pressure and water vapour profiles

Vertical profiles of temperature, pressure and water vapour were taken from worldwide radiosoundings, covering a wide range of natural variations. Since the averaging of these profiles would yield unrealistic, smooth profiles, 12 profiles were chosen empirically, representing a broad range of surface pressure, temperature and water vapour profiles. Figure 3.2 shows these profiles along with their total water vapour column content, ranging from 0.33 to 5.57 g/cm^2. The surface temperature varies between -11.5 to 33.2 °C and surface pressure from 986.9 to 1024.3 hPa. For high surface elevations and the resulting low surface pressure, the coefficients of the proposed water vapour algorithm have to be adapted.

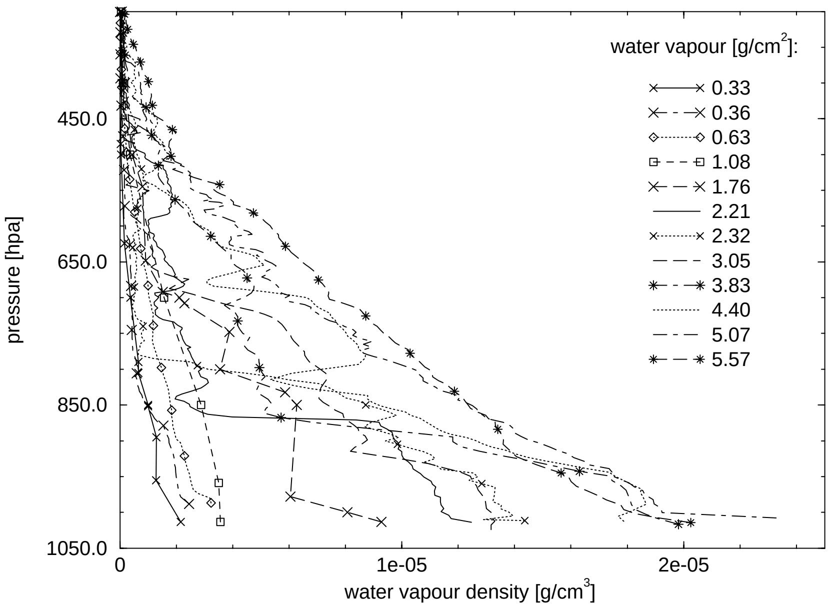

Figure 3.2: Water vapour profiles with total atmospheric water vapour content for radiosoundings used in the simulations.

3.1.1.2.4 Aerosol Optical Parameters

Aerosol types, vertical distribution, and optical depth strongly are varied randomly. Aerosol models were taken from WCP (1986).

Table 3.1: Variations in aerosol parameters

Type	Min. opt. depth	Max. opt. depth
Stratospheric	0.005	0.01
Trop. Background	0.01	0.09
Maritime (ocean)	0.03	0.23
Continental (land)	0.03	0.23

For each simulation three different aerosol types were considered, namely stratospheric, tropospheric background, and maritime (ocean surface) or continental (land surface) aerosol. All three atmospheric constituents were allowed to vary randomly within the natural range of variability, as shown in Table 3.1.

3.1.1.2.5 Spectral Surface Reflectance

The absolute value and the spectral behaviour of the surface reflectance influence the water vapour retrieval. For the present simulations reflectance measurements with high spectral resolution of different targets are taken, whereby the reflectance varies between 10 % and 100 % (Bowker *et al.*, 1985; Krinov, 1953). Different types of vegetation, snow and soil are considered. The surface reflectances depend on wavelength in a nonlinear way. Variations are due to spatially and temporally highly variable parameters as e. g. chlorophyll absorption to plant cellular reflectance ('red edge'), refractive index discontinuities of plant cellular constituents, absorption by iron rich soils, and absorption by solid water or ice constituents (Bowker *et al.*, 1985; Gao *et al.* 1993). Figure 3.3 shows spectral surface reflectivities used in the simulations. There are distinct spectral variations for different types of the considered targets. However, within the range of 880 nm to 910 nm the spectral variation of surface reflectance is considerably small. Since variations in surface albedo for optical thin atmospheres directly result in variations of the measured signal, even small variations in surface albedo slope may cause significant systematic deviations of retrieved water vapour content. To account for variations in surface albedo slope, a simple correction algorithm based on the ratio between MERIS channel 10 (753.75 nm) and channel 14 (890 nm) is proposed.

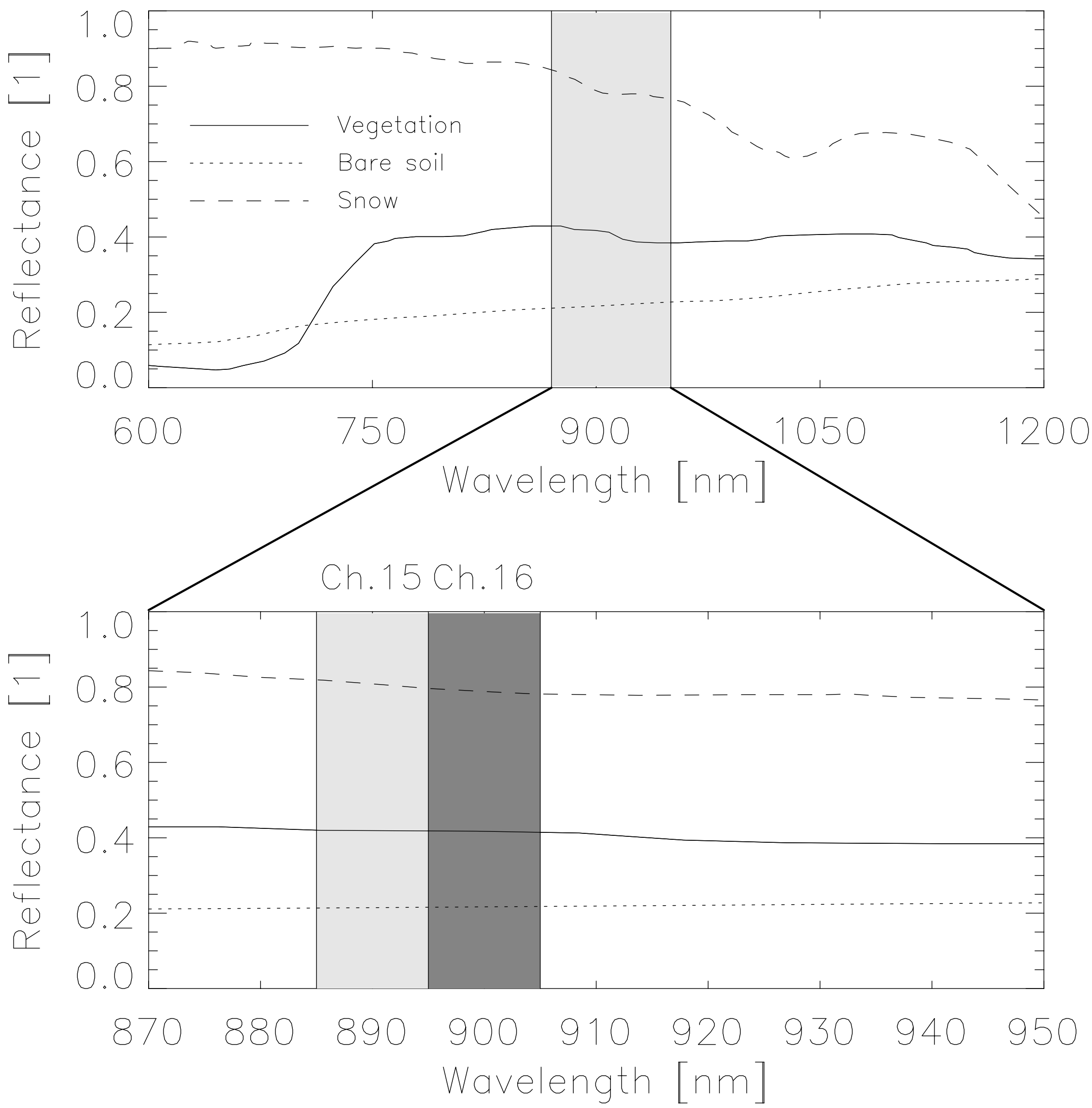

Figure 3.3: Typical reflectance for bare soil, vegetation, and snow (from Bowker et al. 1985)

3.1.1.3 Mathematical description of algorithm

Figure 3.4 gives a schematic overview on the processor architecture and necessary input data for the land and ocean water vapour retrieval modules. The general form of the retrieval kernel is already given in Equation (1). Additional algorithms which are required for the correction of possible error sources (e. g. surface albedo slope over land) are introduced in the subsequent sections.

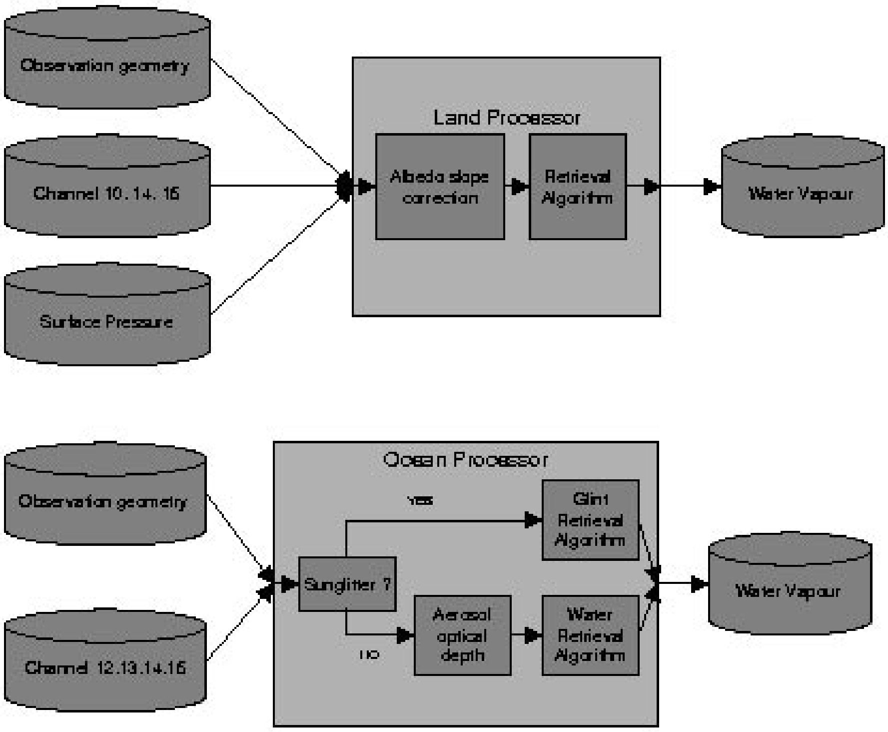

Figure 3.4: Schematic view of MERIS water vapour retrieval processor architecture

3.1.1.3.1 Land algorithm

Besides the actual retrieval of columnar water vapour a correction for surface albedo slope is necessary for those cases where surface albedo at channel 15 deviates to more than 1 % from channel 14 (for details, see section 4.3). The correction algorithm is of the following form:

$$R^{C}_{Ch15/Ch14} = R_{Ch15/Ch14}(s_0 + s_1 R_{Ch14/Ch10} + s_2 R_{Ch15/Ch14}) \qquad (2)$$

is introduced. $R_{ChX/ChY}$ denotes the radiance ratios between MERIS channel x and channel y, s_i are regression constants derived from radiative transfer calculations, and an upper index c denotes the slope corrected radiance ratio. The corrected radiance ratio is subjected to the water vapour retrieval algorithm.

3.1.1.3.2 Ocean algorithm

Within the glitter region, the land surface algorithm without correction can be applied. The accuracy of the ocean algorithm, outside the glitter region, strongly depends on the vertical distribution of aerosols and water vapour. Since no information about these parameters is available, the aerosol optical depth at 900 nm is estimated in order to obtain a minimum information about the scattering intensity of the atmosphere. The aerosol optical depth is used as a further dimension for the regression coefficients of Equation (1). The algorithm proposed for optical depth retrieval writes as:

$$\delta_A = a + bL_{Ch12} + cL_{Ch13} \qquad (3)$$

where a, b, and c again are regression coefficients, δ is the retrieved aerosol optical depth at 900 nm and L_{ChX} are the radiances measured at MERIS channel 12 (775 nm) and channel 13 (865 nm). These are the window channels closest to the water vapour absorption channels. The aerosol optical depth can be retrieved from the above Equation with an absolute accuracy of 0.03.

3.2 Practical considerations

3.2.1 Numerical computation considerations

For all algorithms presented in this ATBD, computation resources are uncritical. Only very few computation steps and no time consuming matrix operations are involved. The size of the data array storing the regression coefficients can be generated from the sizes of the particular dimensions of the regression coefficients given in Table 2.

Table 2: Range and increment for the dimensions of the regression coefficients of Equations (1)-(3).

Dimension	Name	Range	Increment	Number	Land/Ocean
1	Solar zenith angle	15°-80°	2.5°	27	L/O
2	Observer zenith angle	0°-42.5°	2.5°	17	L/O
3	Azimuth	0°-180°	7.5°	25	L/O
4	Aerosol optical depth	0.03-0.6	0.03	20	O
5	Surface pressure	1000-700	50	7	L

The size of an array of regression coefficients may be calculated by multiplying the number of values desired for each dimension (Table 2, row 5) with the size of one regression coefficient (in Bytes). Each regression coefficient for retrieval above ocean surface depends on dimension 1, 2, 3, and 4 and needs *875 Kbyte* considering four bytes to equal one floating point value. For the land algorithm *306 Kbyte* correspond to one regression coefficient for all observation geometries and surface elevations.

3.2.2 Calibration and validation

The overall calibration and validation strategy is visualised in Figure 3.5. Three validation steps are considered necessary to first generate a physical meaningful algorithm and second to correct for systematic deviations of the algorithm results from the actual water vapour content.

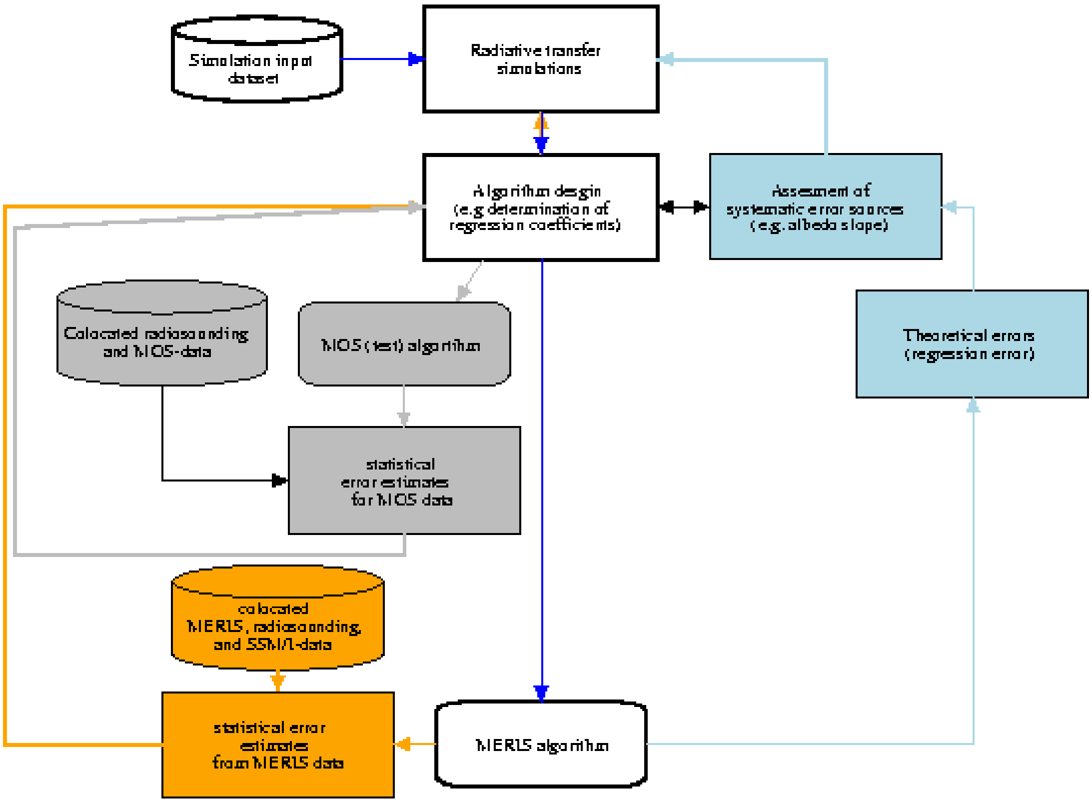

Figure 3.5: Validation strategy for MERIS water vapour retrieval algorithm

Step one includes all required simulation work to implement an algorithm which is consistent with the forward radiative transfer model. This step has already been completed and forms the basis of the here presented ATBD.

Step two embodies a first application to satellite data. The Modular Optical Spectrometer (MOS) onboard the Indian satellite Indsat allows for a pre-launch calibration/validation of the algorithms developed for MERIS. The slightly different channel settings for the MOS water vapour channels (at 865 nm/945 nm) require a re-calibration of the MERIS algorithms to MOS.

In a third step, the post-launch calibration/validation phase, the total water vapour amounts retrieved from MERIS measurements will be compared with water vapour products of the national weather service radiosonde network. The use of ground-based upward-looking microwave radiometer as well as sun photometer measurements for further validation is strongly recommended.

Additional validation aircraft campaigns, including multi-spectral radiance measurements and active water vapour DIAL (DIfferential Absorption Lidar) measurements are necessary to establish the technique for the retrieval of the total water vapour content from future MERIS measurements. Such campaigns should be performed before launch of ENVISAT and at least during a commission phase.

3.2.3 Output product

Output product will be the column amount of atmospheric water vapour over land, water surfaces, and over clouds. The accuracy of the product will be 1.6 kg/m^2 above land surfaces and 2.6 kg/m^2 above water surfaces. The water vapour product will be accompanied by a quality measure, indicating the relative accuracy of the product for a given set of observation angles and other independent variables.

4 Error budget estimates

Within the following subsections the relative impacts of different error sources on the retrieval accuracy is discussed. These investigations are based on simulation studies and absolute values are therefore expected to be slightly different from validation results obtained for observed data.

4.1 Influence of sensor noise

The influence of sensor noise is small for land surfaces. As shown in Figure 4.1 the retrieval results are not affected as long as the signal to noise ratio (SNR) exceeds 75-100. According to the MERIS-specification a SNR better than 200 is expected for land surfaces.
The retrieval results above water surfaces (outside the sun glitter region) are more critical with respect to sensor noise since two effects are superimposed. First, SNR is reduced due to the low signal received from water surfaces. Second, the retrieval algorithms are in general more influenced by variations of atmospheric parameters and are more noise sensitive in general. This sensitivity requires spatial averaging of the retrieved water vapour content. An averaging of the input radiances is not suitable, since the regression coefficients show strongly non-linear dependencies on e. g. aerosol optical depth. Based on the full-resolution dataset *10 x 10* pixels should be averaged.

It has to be mentioned that this averaging is already included in the error estimate for ocean surfaces given in section 3.2.4. The above mentioned rms-error of about 2.6 kg/m^2 is therefore almost independent on sensor noise. Within the sun glitter region, the retrieval accuracy is comparable to that over land surfaces.

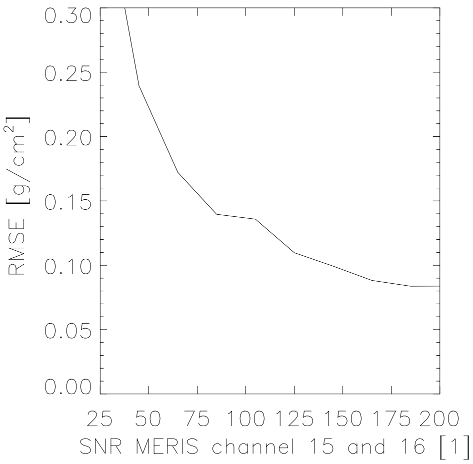

Figure 4.1: Dependence of rms-error on SNR for land surface

4.2 Dependence on observation geometry

Figure 4.2 shows the water vapour retrieval error plotted on the MERIS swath for day 80. For a wide range of observation geometries the rms-error is stable. Only for high solar zenith angles ($\theta_S > 70°$) the rms-error increases drastically.

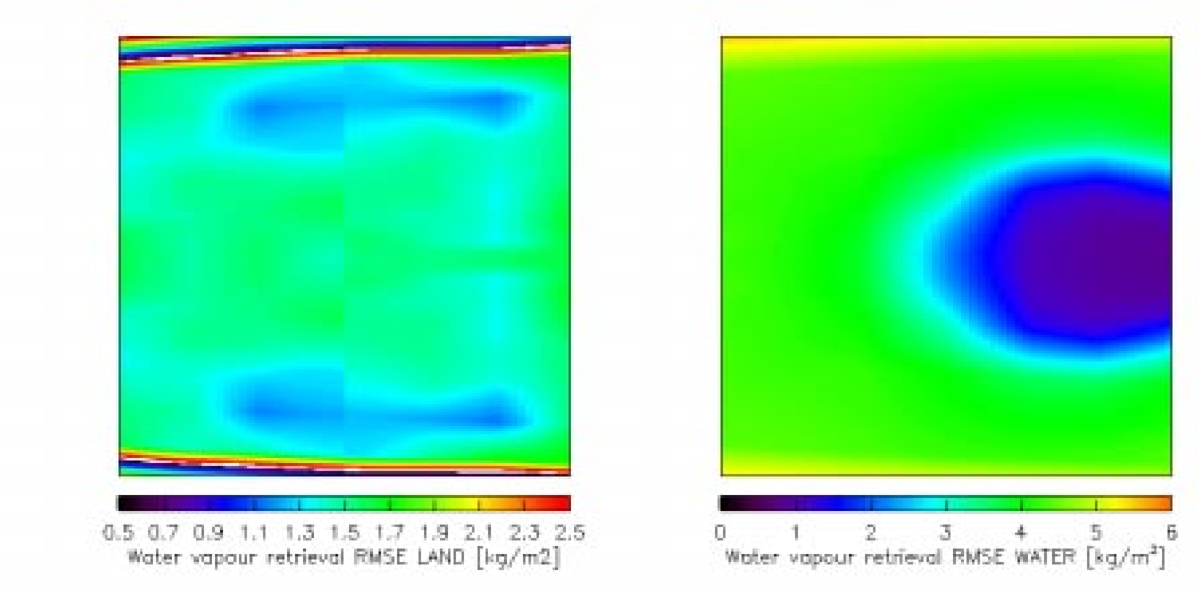

Figure 4.2: Water vapour retrieval error for land (left) and ocean (right), plotted on the MERIS swath for julian day 80. The swath (abscissa) ranges from -585km to 585km of the sub-satellite point. Latitude (ordinates) ranges from 81°S to 74°N. The discontinuity along the sub-satellite track is caused by the interpolation routine

4.3 Influence of surface albedo slope over land surfaces

Radiative transfer simulations for a set 154 different types of surfaces (Bowker *et al.*, 1985) were carried out, in order to estimate the influence of spectral variations in surface albedo on the water vapour retrieval accuracy. The benefits of the proposed correction algorithm (Equation (2)) were quantified by comparing retrieval results with and without correction. While for the uncorrected retrievals the rms-error was 2.2 kg/m^2, the corrected simulations yield rms-errors of 1.65 kg/m^2, including variations due to sensor noise and aerosol.

4.4 Influence of aerosol

A broad range of natural variability of aerosols has been covered in the radiative transfer simulations as outlined in 3.1.1.2.4. The influence of aerosol scattering together with variations of temperature and pressure profiles was evaluated by means of noise-free radiative transfer simulations with constant surface albedo and no surface albedo slope. These simulations yielded rms-errors of about 0.7 kg/m^2, reflecting the in general small influence of variations in atmospheric profiles. The relative error of 1.6 kg/m^2 achieved for land surfaces includes this variations and the resulting product is expected to perform good under all cloud-free atmospheric conditions.

In contrast, the retrieval accuracy over water surfaces, outside the sun glitter region, is strongly affected not only by integral properties of atmospheric scatterers, but also by their vertical distribution. The average retrieval error for ocean surfaces is shown in Figure 4.2 (right). The underlying simulations were performed for 5 m/s surface wind speed whereby the surface reflectivity was calculated according to Cox and Munk (1954). The retrieval results within the sun glitter region are comparable to those obtained over land surfaces, while without the sun glitter region the accuracy is below 2.5 kg/m^2. For Figure 4.2, a noise reduction comparable to a spatial averaging of *10x10* pixels has already been performed.

5 Assumptions and limitations

All algorithms are based on model simulations performed with the one-dimensional radiative transfer model MOMO. Three-dimensional radiative transfer effects are not taken into account, but are considered to be small, unless measurements are taken in the direct vicinity of cloud edges.

The absorption characteristics of water vapour are simulated based on the HITRAN'96 database (Rothmann *et al.*, 1992). Small variations in the parameterisation of water vapour absorption as well as mis-locations of the MERIS-channel settings and deviations of the spectral response functions of MERIS channels 14 and 15 may lead to a bias in the retrieval results. These possible systematic errors will be subject to investigations within the MERIS validation phase. According to simulation studies these errors are anticipated to be smaller than 1.5 kg/m^2.

6 References

Armbruster, W. and J. Fischer, 1996: Improved method of exponential sum fitting of transmission to describe the absorption of atmospheric gaes. Applied Optics, V. 35, .No. 12, 1931-1941.

Adiks, T.G., V. I. Dianov-Klokov, 'Molecular Parameters of the O_2 Absorption Band at 0.762 µm and their Use in Calculating the Transmission Function', Izv., Atmospheric and Oceanic Physics, **4**, No. 10, pp. 1052 - 1059, 1968.

Adiks, T.G. , Yu. S. Georgiyevskiy, M. S. Malekevich, N. S. Filippova, 'Atmospheric Transmission in the 0.76 µm O_2 Band Izv., Atmospheric and Oceanic Physics, **8**, No. 4, pp. 369 - 381, 1972.

Bartsch, B., 1996: Fernerkundung des Wasserdampfgehaltes der Atmosphäre über Land aus rückgestreuter Sonnenstrahlung. Berichte aus dem Zentrum für Meeres- und Klimaforschung, No. 21, 11 pages, Hamburg, Germany.

Bartsch, B. and J. Fischer, 1997: Passive remote sensing of columnar water vapour content over land surfaces. MPI-report No.234, Hamburg, March 1997. ISBN 0937-1060.

Bowker, D. E. , R. E. Davis, D. L. Myrick, and K. Stacy, and W. T. Jones, 'Spectral reflectances of natural targets for use in remote sensing studies', NASA Ref. Publ. 1139, 1985.

Brümmer, B., 'Arktis 1993, Report on the Field Phase with Examples of Measurements', Berichte aus dem Zentrum f¸r Meeres-und Klimaforschung, Reihe A, Nr. 11, Meteorologie, pp. 186, 1993.

Chesters, D., L. W. Uccellini, W. D. Robinson, 'Low-Level Water Vapour Fields from the VISSR Atmospheric Sounder (VAS) 'Split Window' Channels', Journal of Climate and Appl. Meteor., **22**, 725 -742, 1983.

Cox, C. and W. Munk, 1954: Measurements of the roughness of the sea surfacefrom photographs of the sun’s glitter. JOSA, V.44, N0.11, 838-850.

Europäischer Wetterbericht, 'Bodenwettermeldungen', Beilage 1, Jahrgang 18, 1993.

Europäischer Wetterbericht, 'Amtsblatt des Deutschen Wetterdienstes, Aerologische Wettermeldungen', Beilage 2, Jahrgang 18, 1993.

Ehret, G., C. Kiemle, W. Renger, and G. Simmet, 'Airborne Remote Sensing of Tropospheric Water Vapour with a Near-infrared Differential Absorption Lidar System', Appl. Optics, **32**, No. 24, pp. 4534-4551, 1993.

Fell, F. and J. Fischer, 1995: Validation of the FU Berlin radiative transfer model. Final report of the EC-Contract MAS2-VT92-0020. Available via Institute for Space Sciences, Free University of Berlin, Germany.

Fimpel, H., DLR, private communication, 1995.

Fischer, J., 'Fernerkundung von Schwebstoffen im Ozean', Hamburger Geophysika-lische Einzelschriften, Heft 65, 105 pp., 1983.

Fischer, J., ‘High Resolution Spectroscopy for Remote Sensing of Physical Cloud Properties and Water Vapour’, In: Current Problems in Atmospheric Radiation, Ed. Lenoble and Geleyn, Deepak Publishing, 151-156, 1988.

Frouin, R., P.-Y. Deschamps and P. Lecomte, 'Determination from space of atmospheric total water vapour amounts by differential absorption near 940 nm: Theory and airborne verification', J. Appl. Meteor., **29**, 448 - 460, 1990.

Gao, B.-C., A. F. H. Goetz, 1990: Column atmospheric water vapor and vegetation liquid water retrieval from airborne imaging spectrometer data. J. Geophys. Research, Vol. 95, 3549-3564.

Gao, B.-C., A. F. H. Goetz, Ed R. Westwater, J. E. Conel and R. O. Green, "Possible near-IR channels for remote sensing precipitable water vapour from geostationary satellite platforms", J. Appl. Meteor., **32**, 1791 - 1801, 1993.

Graßl, H., 'Strahlung in getrübten Atmosphären und in Wolken', Hamburger Geophysikalische Einzelschriften, Heft 37, 136 pp., 1978.

Hayden, C., 'GOES-VAS Simultaneous Temperature-Moisture Retrieval Algorithm', J. Appl. Meteor., **27**, 705 - 733, 1988.

Hoehne, W., 'Precision of National Weather Service upper air measurements', NOAA Tech. Memo. NWS T&ED-16 [NTIS No. PB81-108136], NOAA National Weather Service, Sterling, VA, pp. 23, 1980.

Koepke, P., M. Hess, I. Schult, E. Shettle, 'Global Aerosol Data Set', in 'IUGG XXI General Assembly, Abstracts Week B', B238, Boulder, Colorado, 1995.

Krinov, E. L., 'Spectral reflectance properties of natural formations', National Research Council of Canada, Technical Translation TT-439, from Aero Methods Laboratory, Academy of Sciences, U.S.S.R., translated by G. Belkov, 1953.

Pflug, B., 'Atmospheric Transmission in the O_2-A-band: Comparison of Calculations and Measurements", Workshop Proceedings 'Atmospheric Spectroscopy Applications' - ASA Reims 93, University of Reims Champagne Ardenne, France, pp. 68 - 71, September 8 - 10, 1993.

Plass, G. N., G. W. Kattawar, F. E. Catchings, 'Matrix Operator Theory of Radiative Transfer. 1: Rayleigh Scattering', Appl. Opt., **12**, No. 2, 314 - 329, 1973.

Ramanathan, V., B. R. Barkstrom, E. F. Harrison, 'Climate and the Earth's radiation budget', Phys. Today, **42**, 22 - 32, 1989.

Rothman, L. S. *et al.*, 'The HITRAN Database: 1986 edition', Appl. Optics, **26**, No. 19, pp. 4058 - 4097, 1987.

Rothman, L. S. *et al.*, 'The HITRAN Molecular Database: Editions of 1991 and 1992', J. Quant. Spectrosc. Radiat. Transfer, **48**, No. 5/6, pp. 469 - 507, 1992.

Rothman, L. S. , private communication, 1995.

Schlüssel, P. and W. J. Emery, 'Atmospheric water vapour over oceans from SSM/I Measurements', Int. J. Remote Sensing, **11**, No. 5, 753 - 766, 1990.

Starr, D. and S. H. Melfi (eds.), 'The Role of Water Vapour in Climate, A Strategic Research Plan for the Proposed GEWEX Water Vapour Project (GVaP)", NASA Conference Publ. 3210, 60 pp., 1991.

Schüller, L., J. Fischer, W. Armbruster, and B. Bartsch, 1997: Calibration of high resolution remote sensing measurements in the visible and near infrared. Adv. Space. Research, Vol. 19, No. 9, 1325-1334.

Susskind, J. , J. Rosenfield and D. Reuter, "Remote sensing of weather and climate parameters from HIRS2/MSU on TIROS-N.", J. Geophys. Res., **89**, 4677 - 4697, 1984.

WCP, 1986: A preliminary cloudless standard atmosphere for radiation computation. WCP-Report 112, WMO/TD-No.24

SUMMARY SHEET

Product Name: total water vapour content
Product Code: MERIS.RRGWVC
Product Level: Level 2
Description of Product: total water vapour content

Product Parameters:
Coverage: global
packaging Half-orbit:
units [kg/m^2]
Range: 1 to 70 kg/m^2
Sampling: pixel by pixel
(if S/N is sufficient only one 300*300 m^2 pixel should be recorded to detect small cumulus clouds - important to atmospheric correction)
Resolution: radiometric: 0.2 $Wm^{-2}sr^{-1}\mu m^{-1}$
spatial: 1.2 *km* (0.3 *km*)
Accuracy radiometric: 2 - 4 % (within precision of calibration)
geophysical product: 10 % relative to amount of water vapour over land surfaces and sun glitter, less than 20% over water surfaces
Geo-location requirements: 1 - 4 pixels, depending on use of cloud-top pressure
Format: 16 bits / sample (TBC)
Appended Data: Earth location, Quality mask (i.e. residual of inversion process)
Frequency: 1 product per orbit
Size of Product: TBC

Additional Information:
Identification of bands used in algorithm: λ = 890 *nm* and λ = 900 *nm, and*
λ = 753 *nm (land surfaces)*
λ = 775 and 865 *nm (water surfaces)*
Assumptions on MERIS input data: error of the refectance ratio < 1%
Identification of ancillary and auxiliary data: land-ocean flag, surface pressure, viewing geometry
Ancillary and auxiliary data:
surface pressure with accuracy of 25-50 hPa.
Input from other ENVISAT instruments:
cloud-flag, cloud top height, cloud optical depth
if available: aerosol optical depth, aerosol type, stratospheric aerosol flag, sun glitter flag.